Study of the Hyperfine Structure of the Low-Lying Ca II and Ra I-II Levels: Applying the MCDHF Models Developed for Ba I-II

Lorenzo Nezosi , Patrick Palmeri * , Per Jönsson

Posted Date: 17 July 2026

doi: 10.20944/preprints202607.1297.v1

Keywords: atomic structure; hyperfine structure; MCDHF method; GRASP package; calcium; radium

 doi:10.20944/preprints202607.1297.v1

Article

Study of the Hyperfine Structure of the Low-Lying Ca II and Ra I-II Levels: Applying the MCDHF Models Developed for Ba I-II

Lorenzo Nezosi [1], Patrick Palmeri [1,*] and Per Jönsson [2]

[1] Physique Atomique et Astrophysique, Université de Mons—UMONS, B-7000 Mons, Belgium
[2] Materials Science and Applied Mathematics, Malmö University, SE-205 06 Malmö, Sweden
* Correspondence: patrick.palmeri@umons.ac.be

Abstract

Building on our previous Multiconfiguration-Dirac-Hartree-Fock (MCDHF) computational strategies taylored for the hyperfine structure (HFS) of low-lying levels in one-valence electron Sr II and Ba II ions, and in two-valence electrons Ba I atom [Nezosi et al, Atoms 14, 17 (2026). DOI: 10.3390/atoms14030017], we successfully extend these methodologies along the alkaline-earth elements to the lighter Ca II and the heavier Ra I-II ions. MCDHF recommended HFS constant with their uncertainty estimates are reported for the first time. This is particularly valuable for cases where no measurement is available such as for the [Rn]$6d\ ^2D_{3/2,5/2}$ levels in ^{223,225}Ra II, for the [Rn]$7s6d\ ^3D_{1,2,3}$ and $^1D_2$ levels in ^{223}Ra I, for the [Rn]$7s6d\ ^3D_{2,3}$ and $^1D_2$ levels in ^{223}Ra I, and for the [Rn]$7s7p\ ^3P^o_2$ level in ^{225}Ra I. In all cases, our MCDHF values agree with the ones found in the literature within our error bars. For the $^2D_{5/2}$ levels in Ca II and Ra II, the discrepancies with experiment observed in Sr II and Ba II for the HFS A constant [Nezosi et al, Atoms 14, 17 (2026). DOI: 10.3390/atoms14030017] are not seen.

Keywords: atomic structure; hyperfine structure; MCDHF method; GRASP package; calcium; radium

1. Introduction

Alkaline-earth metals from Mg to Ra, particularly in their singly ionized forms (e.g., Ca II, Ra II), are ideal for high-precision calculations and measurements in astrophysics and metrology due to their simple electronic structure [1]. Neutral radium (Ra I) is also crucial for beyond-Standard-Model (BSM) physics.

In astrophysics, Ca II infrared triplet lines (8498, 8542, 8665 Å) serve as key calcium abundance indicators in stellar atmospheres, detectable even at extremely low metallicities ($[\mathrm{Fe/H}] \leq -3.0$) [2], enabling studies of metal-poor stars [3] and galactic chemical evolution [4]. Ra II UV-Vis lines (3814, 4682, 6705 Å) probe r-process nucleosynthesis, as Ra is produced exclusively by neutron capture in neutron-rich environments where the s-process ends at bismuth (Z=83) [5,6]. Its likely production in neutron star mergers makes Ra detection in kilonovae spectra a direct indicator of such events [7].

In fundamental physics, Ca II and Ra II are crucial for frequency standards and precision measurements. Quadrupole moments in metastable atomic ions introduce systematic energy shifts in such systems [8]. High theoretical precision ($< 1\%$) is required for meaningful comparisons with parity non-conservation (PNC) experiments [9]. While heavier atoms like Ra offer more favorable PNC conditions, lighter elements such as Ca II serve as essential test cases for validating theoretical methods before tackling heavier systems.

Neutral radium (Ra I) offers unique opportunities for fundamental physics tests. The search for a permanent electron electric dipole moment (EDM) is among the most stringent BSM tests, with polar molecules like RaF serving as exceptionally sensitive probes due to their large internal electric fields and Ra's heavy, octupole-deformed nucleus [10]. Precise *ab initio* calculations for Ra are essential, providing wavefunctions needed to interpret molecular EDM measurements and

 doi:10.20944/preprints202607.1297.v1

constrain CP-violating interactions. Multiconfiguration Dirac-Hartree-Fock (MCDHF) calculations for Ra I address this by capturing critical enhancement mechanisms, notably the [Rn]$7s7p\ ^3P^o_1$ and [Rn]$7s6d\ ^3D_2$ levels, separated by only 5.41 cm^{-1}. Combined with Ra high atomic number ($Z = 88$) and nuclear octupole deformation, this yields P- and T-reversal-odd effect enhancements up to five orders of magnitude greater than in other systems [11,12]. Electron correlation effects, which dominate the atomic EDM signal, are systematically accounted for in combination of MCDHF and relativistic configuration interaction (MCDHF+RCI) calculations. Ra II, with its 8230 Å clock transition and narrow linewidth, is also a candidate for optical atomic clocks. The low-cost diode lasers required for Ra II, compared to expensive UV lasers, make it attractive for both laboratory and transportable applications [13].

Accounting for the hyperfine structure (HFS) of the levels is essential. In astrophysics and atomic clock applications, HFS broadening and the resulting asymmetries in line profiles introduce inaccuracies in line positions and strengths. For BSM research, HFS constants enable extraction of electric field gradients to calibrate molecular theory against high-resolution RaF spectroscopy at ISOLDE (CERN), where 14 excited states have been characterized with 99.6% theory-experiment agreement and laser-coolable transitions identified [10]. Accurate ab initio atomic wavefunctions and correlation energies could enhance RaF sensitivity to e-EDM searches, where experimental data are scarce.

For Ca II, Ra II, and Ra I, the HFS of certain levels remain experimentally unstudied, including the [Rn]$6d\ ^2D_{3/2,5/2}$ levels in ^{223,225}Ra II (where only relativistic coupled cluster (RCC) calculations exist [14]) and the [Rn]$7s6d\ ^3D_{1,2,3}$ levels in Ra I. While extensive MCDHF calculations exist for Mg II [15], Ca II [8], Sr II, and Ba II [16], comprehensive calculations for Ra I-II remain limited. Combined with RCI in GRASP [17], the MCDHF method is particularly effective for relativistic atomic structure, especially when electron correlation is significant. In some of these MCDHF HFS calculations [15,16] along with another recent one dedicated to In I [18], the effects of natural orbitals (NO) have been investigated and, in some cases, these have improved the computed HFS constants. This work presents the first use of natural orbitals for hyperfine structure calculations in heavy Ra I-II.

This paper is organized as follows. Section 2 describes the MCDHF and RCI methods for calculating HFS constants and provides details about the transformation to natural orbitals. Section 3 presents Ca II calculations to validate the theoretical method from the earlier Sr II/Ba II study [16], followed by Ra II and Ra I HFS studies. Section 4 concludes with an outlook.

2. Method and Computational Details

2.1. Multiconfiguration Dirac–Hartree–Fock Method

MCDHF, as described in [19], is a fully relativistic method for atomic structure calculation, well suited for moderate to heavy elements and highly charged ions. In this approach, the wave function for an atomic state $|\Gamma\pi JM_J\rangle$ defined by its label Γ, total angular momentum J, magnetic quantum number M_J and parity π, is represented by an Atomic State Function (ASF) $\Psi(\Gamma\pi JM_J)$. This ASF is constructed as a linear combination of Configuration State Functions (CSFs) $\Phi(\gamma_i\pi JM_J)$

$$\Psi(\Gamma\pi JM_J) = \sum_{i=1}^{N_{\mathrm{CSFs}}} c_i^{\Gamma\pi J}\Phi(\gamma_i\pi JM_J), \tag{1}$$

where each γ_i specifies the electronic configuration, angular momentum coupling tree and other quantum numbers required to uniquely define the CSF.

The mixing coefficients $\{c_i^{\Gamma\pi J}\}$ and the total energy E are determined by solving the eigenvalue problem

$$\boldsymbol{Hc} = E\boldsymbol{c}, \tag{2}$$

 doi:10.20944/preprints202607.1297.v1

with $\boldsymbol{H}$ the Hamiltonian matrix. By applying the variational principle to an energy functional, the method yields the MCDHF equations, a system of coupled integro-differential equations, solved self-consistently for the radial components of the spin-orbitals.

An RCI calculation consists of solving eq. (2) extending the CSF basis, or not, by using frozen orbitals obtained from a preceding MCDHF optimization step. At this stage, higher-order relativistic interactions can be added to the Hamiltonian, such as the Breit interaction and quantum electrodynamics (QED) corrections.

2.2. Natural Orbitals

Due to numerical convergence challenges, and to reduce computation time, the MCDHF method employs a layer-by-layer (LBL) [20] approach in which only the newly introduced orbitals for the layer considered are optimized while the remaining are kept frozen. Therefore, the frozen orbitals, especially the spectroscopic reference orbitals, cannot react to the addition of the newly introduced layer. Natural orbitals (NO) provide an alternative orbital basis, first introduced in quantum chemistry, that addresses this limitation. They modify the orbitals of the reference states in a way that partly captures the response to the new layers. The NOs are obtained by diagonalizing the density matrix, which provides a more natural description of the electron correlation. One of the first applications to atomic physics was by Lindgren et al. [21] in order to determine hyperfine interaction in alkali atoms in many-body perturbation calculations. Schiffmann et al. [22] developed the NO formalism in the MCDHF framework and applied it in the hyperfine structure calculation of Na I [23], exhibiting results in better agreement with experiment than using the traditional LBL approach. Transformation to NOs also showed to considerably improve the hyperfine interaction constants and transition rates in other systems, e.g., In I [18].

For each value of κ, the relativistic angular quantum number, the density matrix is built such as

$$\boldsymbol{\rho}^{\kappa} = \rho^{\kappa}_{nn'}, \tag{3}$$

with

$$\rho^{\kappa}_{nn'} = \sum_{ij} c_i^{\star} v^{ij,\kappa}_{nn'} c_j, \tag{4}$$

where $v^{ij}_{nn'\kappa}$ are the spin-angular coefficients. The NOs $\tilde{\boldsymbol{\phi}} = \tilde{\phi}_{n\kappa}$ are obtained from the eigenvectors $\boldsymbol{U}^{\kappa}$ of the density matrix diagonalizing it

$$\boldsymbol{U}^{\kappa\dagger}\boldsymbol{\rho}^{\kappa}\boldsymbol{U}^{\kappa} = \tilde{\boldsymbol{\rho}}^{\kappa}, \tag{5}$$

$$\tilde{\boldsymbol{\phi}}^{\kappa} = \boldsymbol{\phi}^{\kappa}\boldsymbol{U}^{\kappa}, \tag{6}$$

where the eigenvalues are the occupation numbers $\eta^{\kappa}_{n'}$ of the NOs

$$\sum_{\kappa}\sum_{n'} \eta^{\kappa}_{n'} = N_e,\ 0 \leq \eta^{\kappa}_{n'} \leq 1, \tag{7}$$

with N_e the number of electrons. The large and the small components of the radial function of the NOs are therefore

$$\begin{aligned} \tilde{P}_{n'\kappa}(r) &= \sum_{n} u^{\kappa}_{nn'} P_{n\kappa}(r), \\ \tilde{Q}_{n'\kappa}(r) &= \sum_{n} u^{\kappa}_{nn'} Q_{n\kappa}(r), \end{aligned} \tag{8}$$

with the coefficients $u^{\kappa}_{nn'}$ the matrix elements of the unitary matrix $\boldsymbol{U}^{\kappa}$ in eq. (5) and $P_{n\kappa}(r)$, $Q_{n\kappa}(r)$ the large and the small components of the radial function in the MCDHF equations [19].

 doi:10.20944/preprints202607.1297.v1

2.3. Hyperfine Structure

The HFS of a fine structure level is caused by the interaction between the electrons and the electromagnetic multipole moments of the nucleus. This interaction can be expressed as a multipolar expansion

$$H_{\rm HFS} = \sum_{k\geq 1} \boldsymbol{T}^{(k)} \cdot \boldsymbol{M}^{(k)}, \tag{9}$$

where $\boldsymbol{T}^{(k)}$ and $\boldsymbol{M}^{(k)}$ are spherical tensor operators of rank k in the electronic and nuclear space. For $k = 1, 2$ these operators correspond to the magnetic (M1) and quadrupole electric (E2) interactions. For an atom composed of N_e electrons, the $\boldsymbol{T}^{(k)}$ operators for these values of k are given by

$$\boldsymbol{T}^{(1)} = \sum_{j=1}^{N_e} \boldsymbol{t}^{(1)}(j) = \sum_{j=1}^{N_e} -i\sqrt{2}\alpha r_j^{-2}(\boldsymbol{\alpha}_j \cdot \boldsymbol{C}^{(1)}(\theta_j, \varphi_j)), \tag{10}$$

$$\boldsymbol{T}^{(2)} = \sum_{j=1}^{N_e} \boldsymbol{t}^{(2)}(j) = \sum_{j=1}^{N_e} -r_j^{-3}\boldsymbol{C}^{(2)}(\theta_j, \varphi_j), \tag{11}$$

where $i^2 = -1$ and $\boldsymbol{\alpha}$ are three-component vectors of 4×4 matrices related to the 2×2 Pauli matrices.

The nuclear magnetic dipole moment μ_I and the electric quadrupole moment Q are defined through the matrix elements of the nuclear tensor operators $\boldsymbol{M}^{(k)}$ for $k = 1, 2$, respectively,

$$\mu_I = \langle II|M^{(1)}|II\rangle, \tag{12}$$

$$Q = 2\langle II|M^{(2)}|II\rangle, \tag{13}$$

with $\boldsymbol{M}^{(1)} \equiv \boldsymbol{\mu_I}$, $\boldsymbol{M}^{(2)} \equiv \boldsymbol{Q}^2$ being the electric quadrupole tensor and $|II\rangle$ being the nuclear state with the maximum component of the nuclear spin, $M_I = I$ [24].

If the hyperfine interaction is weak in comparison with the fine structure level splitting, the Hamiltonian (9) can be treated perturbatively. The first-order energy contribution is

$$E_{\rm HFS} = \langle \Gamma JIFM_F|H_{\rm HFS}|\Gamma JIFM_F\rangle = E^{\rm M1}_{\rm HFS} + E^{\rm E2}_{\rm HFS}, \tag{14}$$

where $|\Gamma IJFM_F\rangle$ is the zeroth-order wave function of the coupled state [20], and F and M_F are, respectively, the hyperfine structure total angular momentum and its projection along the quantization axis.

In practice, the magnetic dipole A and the electric quadrupole B hyperfine structure constants are factorized out from the energy expressions yielding

$$E^{\rm M1}_{\rm HFS} = \frac{1}{2}A_{\Gamma J}C \tag{15}$$

$$E^{\rm E2}_{\rm HFS} = B_{\Gamma J}\frac{\frac{3}{4}C(C+1) - I(I+1)J(J+1)}{2I(2I-1)J(2J-1)}, \tag{16}$$

where

$$A_{\Gamma J} = \frac{\mu_I}{I}\frac{1}{J(J+1)2(J+1)}\langle \Gamma J||\boldsymbol{T}^{(1)}||\Gamma J\rangle \tag{17}$$

$$B_{\Gamma J} = 2Q\sqrt{\frac{J(2J-1)}{(J+1)(2J+1)(2J+3)}}\langle \Gamma J||\boldsymbol{T}^{(2)}||\Gamma J\rangle, \tag{18}$$

and $C = F(F+1) - J(J+1) - I(I+1)$. The reduced matrix elements $\langle \Gamma J||\boldsymbol{O}^{(k)}||\Gamma J\rangle$, with $\boldsymbol{O}^{(k)} = \boldsymbol{T}^{(1)}$ or $\boldsymbol{T}^{(2)}$, are computed using the ASFs given by eq. (1).

 doi:10.20944/preprints202607.1297.v1

2.4. Computational Details

The MCDHF calculations and the evaluation of the HFS constants are carried out using GRASP2018 [25,26]. Within this framework, the rdensity program [22] is employed to construct the NO basis. To reduce computational time, the newly developed GRASPG package by Si et al. [27], which uses Configuration State Function Generators (CSFGs), is adopted for the RCI part of the calculations.

Following the approach introduced by Papoulia et al. [28] and applied to Sr and Ba by Nezosi et al. [16], each HFS constant is given in the form of a recommended value obtained by treating the results of the largest RCI calculations for different optimization strategies as a set of independent values. This approach enables us to give a mean value and a standard deviation to the calculated constant, providing a robust estimate of the HFS constants with an uncertainty evaluation, which is crucial when experimental data is missing. The recommended values are presented as $\mu \pm 2\sigma$, corresponding to a 95% confidence interval.

3. Results and Discussion

3.1. Ca II

Calcium (Ca) has 26 known isotopes, of which 5 are stable [29]. ^{43}Ca has an abundance of only 0.135% but is the only stable isotope that has a hyperfine structure due to its non-zero nuclear spin ($I = 7/2$). The levels of interest in ^{43}Ca II are the even [Ar]$4s\ ^2S_{1/2}$ and [Ar]$3d\ ^2D_{3/2,5/2}$ as well as the odd [Ar]$4p\ ^2P^o_{1/2,3/2}$.

Due to its relatively simple electronic structure, ^{43}Ca II has already been studied in depth both theoretically by Silverans et al. [30] and Yu et al. [31] using the Relativistic Many-Body Perturbation Theory (RMBPT) approach and Itano [8] with the MCDHF method, and experimentally by Goble et al. [9] and Nortershauser et al. [1] using optical spectroscopy with hollow cathode discharge and fast ion beam collinear laser spectroscopy.

The MCDHF method used in this paper relies on the AS [20] and LBL [26] approaches, which enable the optimization of only a subset of orbitals at each calculation step. For example, for the ground $^2S_{1/2}$ level, an initial Dirac-Hartree-Fock (DHF) layer is considered. This layer is built using the $\{4s, 3p\}$ spectroscopic orbitals in nonrelativistic notation, where the highest n quantum number is quoted for each l-symmetry, and no electron correlation is included at this stage. The ASs are then expanded with correlation orbitals up to $l_{\max} = 4$ (g-orbitals) to directly apply the Ba/Sr model [16] and achieve high precision in the calculations [32]. For each AS given in Table 1, only the newly introduced orbitals are optimized, while the remaining orbitals are kept frozen. The mixing coefficients of the ASFs are then determined, and Quantum Electrodynamics (QED) corrections are included at the RCI step. Finally, the HFS constants are computed.

Table 1. Considered active sets used for the levels studied in ^{43}Ca II

Correlation layer	$^2S_{1/2}$	$^2D_{3/2,5/2}$	$^2P^o_{1/2,3/2}$
DHF	$\{4s, 3p\}$	$\{3s, 3p, 3d\}$	$\{3s, 4p\}$
AS1	$\{5s, 4p, 3d\}$	$\{4s, 4p, 4d, 4f\}$	$\{4s, 5p, 3d\}$
AS2	$\{6s, 5p, 4d, 4f\}$	$\{5s, 5p, 5d, 5f, 5g\}$	$\{5s, 6p, 4d, 4f\}$
AS3	$\{7s, 6p, 5d, 5f, 5g\}$	$\{6s, 6p, 6d, 6f, 6g\}$	$\{6s, 7p, 5d, 5f, 5g\}$
AS4	$\{8s, 7p, 6d, 6f, 6g\}$	$\{7s, 7p, 7d, 7f, 7g\}$	$\{7s, 8p, 6d, 6f, 6g\}$
AS5	$\{9s, 8p, 7d, 7f, 7g\}$	$\{8s, 8p, 8d, 8f, 8g\}$	$\{8s, 9p, 7d, 7f, 7g\}$
AS6	$\{10s, 9p, 8d, 8f, 8g\}$	$\{9s, 9p, 9d, 9f, 9g\}$	$\{9s, 10p, 8d, 8f, 8g\}$
AS7	$\{11s, 10p, 9d, 9f, 9g\}$	$\{10s, 10p, 10d, 10f, 10g\}$	$\{10s, 11p, 9d, 9f, 9g\}$

Following Bieroń et al. [33], the impact of different classes of orbital substitutions has been investigated. Using an DHF orbital basis, more correlations are accumulated by allowing single and

 doi:10.20944/preprints202607.1297.v1

double (SD) substitutions from deeper orbitals employing Single References (SR) for each level using the fourth correlation layer (AS4) given in Table 1.

In Table 2, the individual contribution of single (S) orbital substitution to the magnetic dipole HFS constant of the ground level, $A(^2S_{1/2})$, is presented. Figure 1 gives a more visual representation of these contributions.

Table 2. Contributions from occupied orbitals to the calculated values of A hyperfine constant for the $^2S_{1/2}$ level of ^{43}Ca II. ΔA shows the individual contribution coming from the single (S) orbital substitutions.

Orbital	N_{CSFs}	A (MHz)	ΔA
	1	−606.08	
$3p$	32	−604.24	+0.08
$3s$	2377	−685.78	−81.54
$2p$	4303	−669.77	+15.79
$2s$	12455	−679.77	−9.78
$1s$	16468	−687.26	−7.49

While the contribution of the $3p$ orbital is negligible, +0.08 MHz, the s orbital substitutions dominate, with the $3s$ orbital contributing −81.54 MHz. This highlights the critical role of s single substitutions in the HFS. To align with the Ba/Sr methodology [16], the $2p$ and $2s$ orbitals are included in the optimization step, even though the $2s$ substitution contributes less than a percent. Consequently, $1s$ correlations are excluded from the optimization.

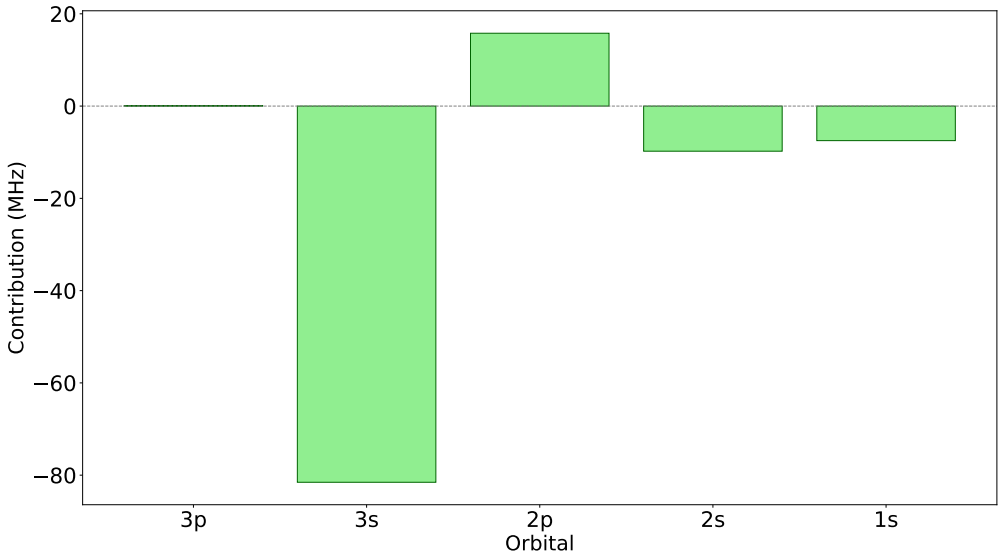

Figure 1. Contributions of single (S) orbital substitutions relative to the DHF $A(^2S_{1/2})$ constant in ^{43}Ca II.

As shown in Table 3 and Figure 2, the contributions for the excited states are similar, with the $3p$ contribution being negligible compared to the $3s, 2p$ and $2s$ ones. The contributions for the B hyperfine constants indicate that the most important contribution comes from $2p$ correlations, which is mainly due to the orbital polarization or Sternheimer effect [24]. The trends above are also observed in the $^2D_{5/2}$ and the odd P levels.

 doi:10.20944/preprints202607.1297.v1

Table 3. Contributions from occupied orbitals to the calculated values of A and B hyperfine constants for the $^2D_{3/2}$ level of ^{43}Ca II. Δ columns show the individual contribution to the HFS constant coming from the single (S) orbital substitutions.

Orbital	N_{CSFs}	A (MHz)	ΔA	B (MHz)	ΔB
	1	−34.31		−2.30	
3p	153	−33.96	+0.36	−2.27	+0.02
3s	8201	−41.78	−7.82	−2.17	+0.11
2p	14737	−37.33	+4.45	−2.78	−0.61
2s	44884	−39.56	−2.23	−2.65	+0.13
1s	58688	−39.96	−0.40	−2.65	+0.00

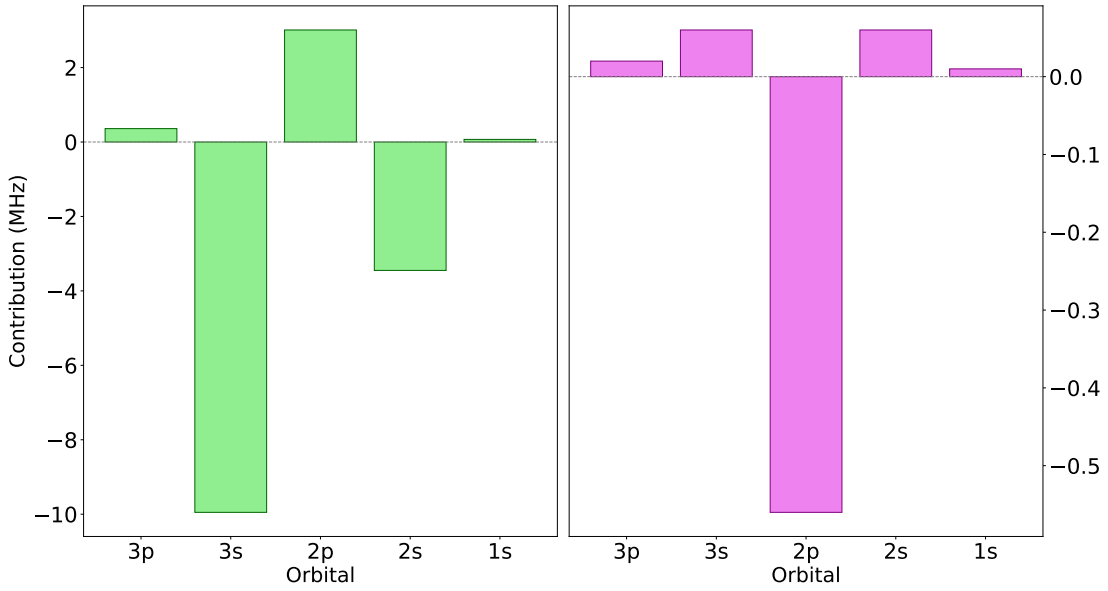

Figure 2. Contributions of single (S) orbital substitutions relative to the DHF $A(^2D_{3/2})$ (left, in light green) and $B(^2D_{3/2})$ (right, in violet) constants in ^{43}Ca II.

Thanks to this analysis, the optimization of the radial orbitals can be aimed for relevant correlations for the hyperfine structure. The GRASP package [25] is considering spectroscopic orbitals in two ways. Let us take the example of the ground $1s^22s^22p^63s^23p^64s\ ^2S_{1/2}$ (or [Ar]$4s\ ^2S_{1/2}$) level. The core orbitals are $1s^22s^22p^63s^23p^6$, while the valence orbital is 4s. We can therefore build our MCDHF optimizations on core-valence (CV) correlations. To directly apply the MCDHF+RCI model developed for ^{87}Sr II and ^{137}Ba II [16], we used the equivalent CV single and restricted double (SrD) orbital optimization strategy with $nl \geq 3s$ substitutions. Here, "restricted" means at most one hole per active core orbital, i.e., allowing substitutions from $3s^2$ and $3p^6$ to 4s with at most one substitution from each core orbital to the valence one [34]. A second optimization strategy (MCDHF CV SrD $nl \geq 2s$) taking care of the 2s and 2p core orbitals that are important to correctly describe the HFS for the excited levels was also considered. With the ASs described in Table 1, seven layers of correlation orbitals were considered in order to achieve a convergence in our results. The latter is obtained when the HFS constants do not vary within some a priori accepted variation interval. Results for the HFS constants at each optimization step are given in Table 4.

As expected, CV correlations are crucial to describe the hyperfine interaction. The MCDHF CV SrD $nl \geq 3s$ shows a stable value achieved for the fourth active set (AS4). The ground level already agrees with experiment to within 3.5 MHz (0.4%). This agreement is observed for each HFS constant except the $A(^2D_{5/2})$ value with a persisting 8 MHz difference (216%). This behavior is well known from the Sr/Ba study [16]. To try to overcome this discrepancy, the second orbital set, MCDHF CV SrD

 doi:10.20944/preprints202607.1297.v1

$nl \geq 2s$ is considered. The agreement worsens for all HFS constants but is improved for the $A(^2D_{5/2})$ constant that still shows a 3 MHz ($\approx 84\%$) difference.

Following MCDHF calculations, deeper core-core (CC) correlations are added in the RCI step. The first RCI CC SD $nl \geq 3s$ model allows SD substitutions from $3p$ and $3s$ orbitals to the valence orbital, with no substitutions between the core orbitals in order to save computational time by decreasing the number of CSFs by a factor of two. As we want to account for as much correlation as possible, a second RCI strategy based on CC SD $nl \in \{3p, 3s, 2p, 2s\}$ substitutions is considered. Adding correlations from the $1s$ core orbital was shown to be negligible, with less than a percent change in the values for the ground level. Therefore, they were also omitted. Using the MCDHF CV SrD nl$\geq 3s$ optimization, the extended RCI CC SD $nl \in \{3p, 3s, 2p, 2s\}$ model modifies the electric quadrupole A hyperfine constants by $\approx 5\%$ for the ground level. The largest change appears for $A(^2D_{5/2})$ which varies by $\approx 60\%$. For the magnetic dipole B constant, we observe shifts of $\approx$ 1MHz for the D levels, while $B(^2P^o_{3/2})$ remains unchanged. The second MCDHF CV SrD $nl \geq 2s$ optimization yielded identical results with the same RCI approach.

In order to give an uncertainty estimate to the theoretical HFS values, Papoulia et al. [28] introduced a statistical approach. By treating each of the largest RCI calculations for different MCDHF optimizations as independent, a mean value and a standard deviation can be obtained. The final value, given in the form $\mu \pm 2\sigma$ showing a 95% confidence level, shows a great agreement with experimental values and is close to other theoretical studies. The largest discrepancy is still the $A(^2D_{5/2})$ with a 24% difference with Nortershauser et al. experiments [1]. It is, however, smaller than the difference observed in Sr II and Ba II [16]. This difference in behavior may be attributed to the absence of d core orbitals in Ca II. Numerical truncation can cause some final $\mu \pm 2\sigma$ values to be reported with $2\sigma = 0$, which should not be interpreted as exact precision. For example, the RCI CC SD $nl \in \{3p, 3s, 2p, 2s\}$ calculations from both MCDHF optimizations yield a difference of only ≈ 0.0062 resulting in a final $2\sigma \approx 0.0087 \approx 0$ MHz.

doi:10.20944/preprints202607.1297.v1

Table 4. Magnetic dipole A and electric quadrupole B hyperfine structure constants (in MHz) of ^{43}Ca II ($I = 7/2, \mu = -1.31733\mu_N, Q = -0.0408$ b [35]), compared to available theoretical and experimental data. The recommended values are given in the form of $\mu \pm 2\sigma$, exhibiting a 95% confidence level. *: Number of CSFs obtained after reduction using the rcsfginteract_csfg code; [a]: Th. Silverans et al. (RMBPT) [30]; [b]: Th. Yu et al. (RMBPT) [31]; [c]: Th. Itano (MCDHF) [8]; [d]: Expt. Goble et al. [9]; [e]: Expt. Nortershauser et al. [1]

Step	$^2S_{1/2}$		$^2D_{3/2}$			$^2D_{5/2}$			$^2P^o_{1/2}$		$^2P^o_{3/2}$		
	N_{CSFs}	A	N_{CSFs}	A	B	N_{CSFs}	A	B	N_{CSFs}	A	N_{CSFs}	A	B
Optimization CV SrD $nl \geq 3s$													
DHF	1	−606	1	−34	−2	1	−15	−3	1	−109	1	−21	−4
MCDHF (+AS1)	37	−741	120	−46	−2	130	−12	−2	53	−133	74	−26	−6
MCDHF (+AS2)	152	−774	433	−49	−2	496	−12	−3	181	−142	278	−33	−6
MCDHF (+AS3)	380	−802	944	−51	−2	1,100	−12	−3	423	−145	688	−34	−6
MCDHF (+AS4)	722	−797	1,653	−51	−2	1,942	−13	−3	781	−146	1,300	−34	−6
MCDHF (+AS5)	1,178	−801	2,560	−51	−2	3,022	−12	−3	1,255	−147	2,114	−34	−6
MCDHF (+AS6)	1,748	−800	3,665	−51	−2	4,340	−12	−3	1,845	−147	3,130	−34	−6
MCDHF (+AS7)	2,432	−801	4,968	−51	−2	5,896	−12	−3	2,551	−147	4,348	−34	−6
RCI CC SD $nl \geq 3s$ (+AS7)	9,407*	−738	27,462*	−45	−2	38,541*	−9	−3	9,825*	−125	23,013*	−29	−5
RCI CC SD $nl \in \{3p, 3s, 2p, 2s\}$ (+AS7)	18,806*	−764	54,916*	−45	−3	77,074*	−5	−4	19,642*	−131	46,018*	−31	−6
RCI CC SD $nl \geq 3s$ (+AS7, NO)	9,407*	−765	27,462*	−47	−2	38,541*	−10	−3	9,825*	−127	23,013*	−29	−5
RCI CC SD $nl \in \{3p, 3s, 2p, 2s\}$ (+AS7, NO)	18,806*	−811	54,916*	−48	−3	77,074*	−5	−4	19,642*	−133	46,018*	−31	−6
Optimization CV SrD $nl \geq 2s$													
DHF	1	−606	1	−34	−2	1	−15	−3	1	−109	1	−21	−4
MCDHF (+AS1)	72	−746	238	−46	−2	258	−10	−3	104	−135	146	−26	−6
MCDHF (+AS2)	301	−783	863	−50	−3	989	−9	−4	359	−145	553	−33	−6
MCDHF (+AS3)	756	−841	1,884	−52	−3	2,196	−7	−4	842	−156	1,372	−36	−7
MCDHF (+AS4)	1,439	−845	3,301	−53	−3	3,879	−7	−4	1,557	−158	2,595	−37	−7
MCDHF (+AS5)	2,350	−854	5,114	−53	−3	6,038	−7	−4	2,504	−159	4,222	−38	−7
MCDHF (+AS6)	3,489	−855	7,323	−53	−3	8,673	−7	−4	3,682	−159	6,253	−38	−7
MCDHF (+AS7)	4,856	−854	9,928	−53	−3	11,784	−7	−4	5,094	−160	8,688	−38	−7
RCI CC SD $nl \geq 3s$ (+AS7)	11,831*	−783	32,422*	−47	−3	44,429*	−5	−4	12,368*	−136	27,353*	−32	−6
RCI CC SD $nl \in \{3p, 3s, 2p, 2s\}$ (+AS7)	18,806*	−761	54,916*	−44	−5	77,074*	−5	−4	19,642*	−131	46,018*	−30	−6
RCI CC SD $nl \geq 3s$ (+AS7, NO)	11,831*	−816	32,422*	−49	−3	44,429*	−5	−4	12,368*	−136	27,353*	−32	−6
RCI CC SD $nl \in \{3p, 3s, 2p, 2s\}$ (+AS7, NO)	18,806*	−811	54,916*	−48	−3	77,074*	−5	−4	19,642*	−133	46,018*	−31	−6
This work (LBL)		-763 ± 4		-45 ± 1	-4 ± 3		-5 ± 0	-4 ± 0		-139 ± 21		-33 ± 4	-6 ± 0
This work (NO), recommended		-811 ± 0		-48 ± 0	-3 ± 0		-5 ± 0	-4 ± 0		-133 ± 0		-31 ± 0	-6 ± 0
Th.[a]		−819								−148		−31	−7
Th.[b]		−805		−48	−3		−4	−4		−143		−31	−7
Th.[c]				−47	−3		−5	−4					
Expt.[d]		-797.5 ± 2.4								-158 ± 3.3		-29.7 ± 1.6	
Expt.[e]				-47.3 ± 0.2	-3.7 ± 1.9		-3.8 ± 0.6	-3.9 ± 6.0		-145.4 ± 0.1		-31 ± 0.2	-6.9 ± 1.7

 doi:10.20944/preprints202607.1297.v1

Recent studies by Sahoo et al. [15] and Atalay [18] suggested a different approach for the use of a NO basis for HFS calculations. Compared to Nezosi et al. [16], where the biggest optimized MCDHF orbitals resulting from traditional single and restricted double (SrD) substitutions are transformed to NO using the rdensity program [22], here the NO basis is obtained via S substitutions (with at most one substitution from all core orbitals) from a multireference (MR) for the S, D and P levels studied in this paper. The largest MCDHF optimization calculation following this approach is then transformed to natural orbitals and then used in RCI calculations. This new approach is appealing as it can relax all orbitals in a single, compact calculation, as only a total of 4,196 CSFs was needed compared to the 4,858 CSFs for the MCDHF CV $nl \geq 2s$ optimization only for the $^2S_{1/2}$ HFS calculations at AS7. This approach is especially suitable for high-Z, as the number of CSFs grows rapidly with the number of active orbitals.

At first glance, equations (17,18) show that $A \propto \langle r^{-2} \rangle$ and $B \propto \langle r^{-3} \rangle$. Johnson [36] showed, in the Pauli approximation where the small $Q_{n\kappa}(r)$ and the large $P_{n\kappa}(r)$ can be linked by

$$Q_{n\kappa}(r) \approx -\frac{1}{2c}\left(\frac{d}{dr} + \frac{\kappa}{r}\right) P_{n\kappa}(r), \tag{19}$$

that $\langle r^{-2} \rangle$ is linked to $\langle r^{-3} \rangle$, indicating that the A and B HFS constants are both $\propto \langle r^{-3} \rangle$ in the Pauli approximation.

Any modification in $\langle r \rangle$ caused by the transformation to NO could result in a modification in $\langle r^{-3} \rangle$. Table 5 compares the change in these expectation values for each d-subshell for a layer-by-layer (LBL) calculation and after transformation to NO. The spectroscopic $3d$ orbital is highlighted. Even the smallest change in $\langle r \rangle$ induces variation in $\langle r^{-2} \rangle$ as it can be seen for the $3d$ valence orbital

$$\begin{aligned} \langle r \rangle_{3d}^{\mathrm{LBL}} &= 2.5227\ a_0 \rightarrow \langle r \rangle_{3d}^{\mathrm{NO}} = 2.3033\ a_0, \\ \langle r^{-3} \rangle_{3d}^{\mathrm{LBL}} &= 0.5937\ a_0^{-3} \rightarrow \langle r^{-3} \rangle_{3d}^{\mathrm{NO}} = 0.6947\ a_0^{-3}, \end{aligned} \tag{20}$$

inducing a direct change in $A(^2D_{3/2})$ and $A(^2D_{5/2})$

$$\begin{aligned} A(^2D_{3/2})^{\mathrm{LBL}} &= -51\ \mathrm{MHz} \rightarrow A(^2D_{3/2})^{\mathrm{NO}} = -49\ \mathrm{MHz}, \\ A(^2D_{5/2})^{\mathrm{LBL}} &= -12\ \mathrm{MHz} \rightarrow A(^2D_{5/2})^{\mathrm{NO}} = -11\ \mathrm{MHz}. \end{aligned} \tag{21}$$

Table 5. Comparison of $\langle r \rangle$ (in a_0) and $\langle r^{-3} \rangle$ (in a_0^{-3}) for the $^2D_{3/2,5/2}$ levels of ^{43}Ca II between layer-by-layer (LBL) (MCDHF CV $nl \geq 3s$) and natural orbitals (NO) calculations. The $3d$ spectroscopic orbital is highlighted in grey.

Subshell	$\langle r \rangle$		$\langle r^{-3} \rangle$	
	LBL	**NO**	**LBL**	**NO**
$3d$	2.5227	2.3033	0.5937	0.6947
$4d$	2.3718	2.3325	1.7532	1.5547
$5d$	2.4586	2.9116	2.4162	1.9883
$6d$	2.5629	3.0360	4.7478	5.5875
$7d$	3.0079	3.1761	6.3437	7.0810
$8d$	2.2484	3.8998	12.0424	5.4211
$9d$	5.2031	1.8125	2.4986	23.4276
$10d$	1.5182	5.1953	20.3480	6.1427

The orbital contraction is more visible on Figure 3 between 3 and $6a_0$. The top left graph shows the large component $P_{3d}(r)$ of the valence orbital as a function of r, for the LBL calculation (in blue) and the transformed NO (in dashed red) obtained from the S substitutions MR calculation. The bottom-left graph shows the absolute difference between these two orbital bases. There are multiple zones where the NO valence orbital is more contracted than the LBL one. On the right-hand side, the $[3;6]a_0$ region

 doi:10.20944/preprints202607.1297.v1

is zoomed in where the contraction appears clearly with the red arrow. Even this small contraction (about 3% in this region) can cause a difference in the A HFS constants. The same behavior applies to the valence orbitals of ground and the P excited levels, as well as in the B HFS constants.

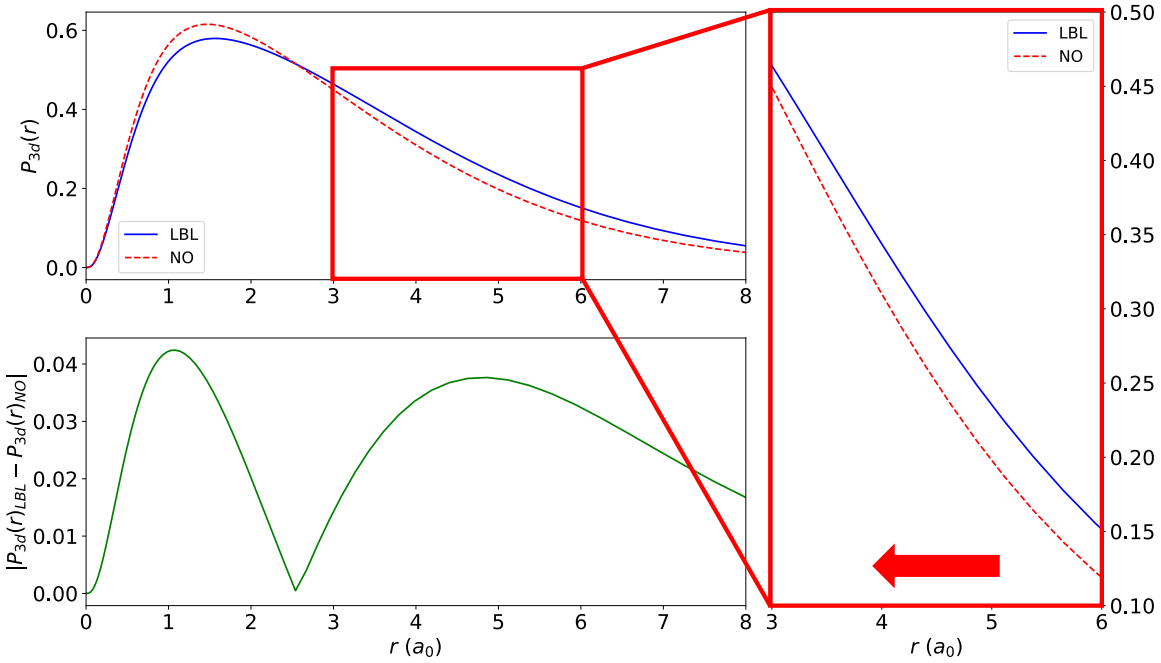

Figure 3. Comparison between the large $P_{3d}(r)$ valence orbital component of the ^{43}Ca II MCDHF CV SrD $nl \geq 3s$ LBL calculation in solid blue, and multireference (MR) with allowed single (S) substitutions from all core orbitals transformed to natural orbitals (NO) in dashed red (top-left corner). The absolute difference $|P_{3d}(r)_{\mathrm{LBL}} - P_{3d}(r)_{\mathrm{NO}}|$ given in green (bottom-left corner) shows the NO contraction in multiple areas between 0 and $8a_0$. A zoom is given on the right-hand side, showing more clearly the orbital contraction with the red arrow in the $[3;6]a_0$ region.

Using the NO basis, we repeated all RCI calculations (labeled NO in Table 4). Results for both optimizations differ by only a few MHz. We recommend the final NO values as it accounts for orbital contraction and shows better agreement with experimental values, except for $A(^2P^o_{1/2})$. The broader LBL uncertainties encompass both the experimental value and our NO recommendation.

3.2. Ra II

Radium (Ra) is the heaviest alkaline earth metal, with 34 known radioactive isotopes. The most stable, ^{226}Ra, has a half-life of 1,600 years [29]. The isotopes ^{223}Ra and ^{225}Ra, with nuclear spin $I = 3/2$ and half-lives of 11.44 and 14.82 days respectively, only exist in trace amounts. Their short half-lives make experiments challenging, so theoretical hyperfine structure calculations are needed to provide experimental bounds. The levels of interest are the even [Rn]$7s\ ^2S_{1/2}$ and [Rn]$6d\ ^2D_{3/2,5/2}$ levels, as well as the odd [Rn]$7p\ ^2P^o_{1/2,3/2}$ levels, for which only a few experimental values are available. Using collinear fast-beam laser spectroscopy, Wendt et al. [37] determined the HFS of both $J = 1/2$ levels, while Neu et al. [38] studied both the ground and $^2P^o_{3/2}$ levels. Theoretical values were obtained using RCC [14,39] or Atomic Many-body Perturbation Theory in the Screened Coulomb Interaction (AMPSCI) [40]. This is the first paper to compute HFS constants using the MCDHF and RCI method and to benchmark the new GRASPG [27] package for high-Z ions.

With the AS given in Table 6, the code limited the investigation of orbital substitutions to those no higher than $3d$. Table 7 and Figure 4 show that, for the ground level, the highest contribution comes from $6s$ substitutions. $5d$ and $5p$ substitutions can be added to the optimization model in order to follow the Ba/Sr [16] strategies.

 doi:10.20944/preprints202607.1297.v1

Table 6. Considered active sets used for the levels studied in ^{223}Ra II.

Correlation layer	$^2S_{1/2}$	$^2D_{3/2,5/2}$	$^2P^o_{1/2,3/2}$
DHF	$\{7s,6p,5d,4f\}$	$\{6s,6p,6d,4f\}$	$\{6s,7p,5d,4f\}$
AS1	$\{8s,7p,6d,5f,5g\}$	$\{7s,7p,7d,5f,5g\}$	$\{7s,8p,6d,5f,5g\}$
AS2	$\{9s,8p,7d,6f,6g\}$	$\{8s,8p,8d,6f,6g\}$	$\{8s,9p,7d,6f,6g\}$
AS3	$\{10s,9p,8d,7f,7g\}$	$\{9s,9p,9d,7f,7g\}$	$\{9s,10p,8d,7f,7g\}$
AS4	$\{11s,10p,9d,8f,8g\}$	$\{10s,10p,10d,8f,8g\}$	$\{10s,11p,9d,8f,8g\}$
AS5	$\{12s,11p,10d,9f,9g\}$	$\{11s,11p,11d,9f,9g\}$	$\{11s,12p,10d,9f,9g\}$
AS6	$\{13s,12p,11d,10f,10g\}$	$\{12s,12p,12d,10f,10g\}$	$\{12s,13p,11d,10f,10g\}$
AS7	$\{14s,13p,12d,11f,11g\}$	$\{13s,13p,13d,11f,11g\}$	$\{13s,14p,12d,11f,11g\}$

Table 7. Contributions from occupied orbitals to the calculated values of A hyperfine constant for the $^2S_{1/2}$ level of ^{223}Ra II. ΔA shows the individual contribution coming from the single (S) orbital substitutions.

Orbital	N_{CSFs}	A (MHz)	ΔA
	1	2811.00	
$6p$	33	2810.67	-0.13
$6s$	3321	2973.83	$+163.16$
$5d$	5914	2941.59	-32.24
$5p$	25194	2918.51	-23.08
$5s$	45642	2924.92	$+6.41$
$4f$	54323	2927.97	$+3.05$
$4d$	105167	2909.87	-18.10
$4p$	163867	2900.49	-9.38
$4s$	211495	2900.20	-0.29
$3d$	229830	2922.14	$+21.94$

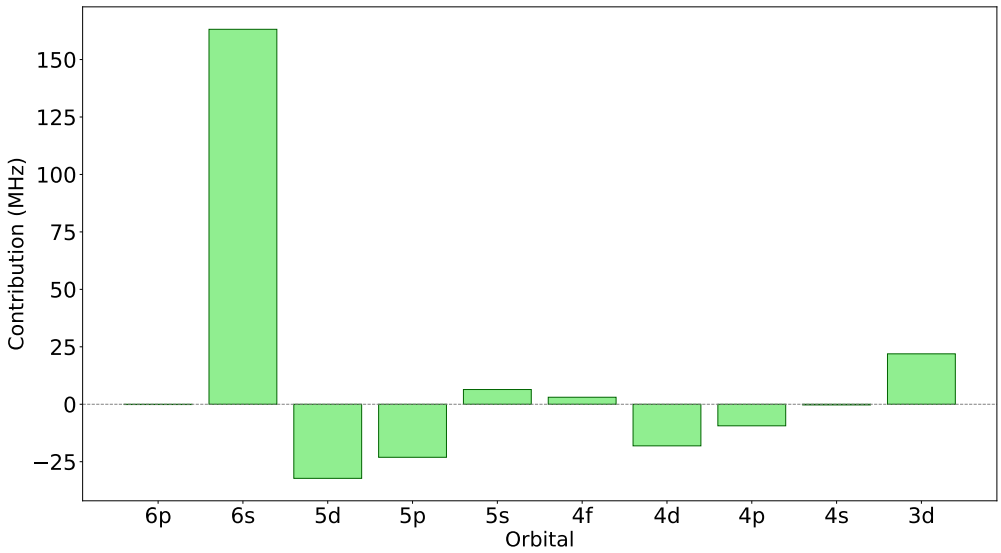

Figure 4. Contributions of single (S) orbital substitutions relative to the DHF $A(^2S_{1/2})$ constant in ^{223}Ra II.

The obtained values for ^{223}Ra II for both optimization strategies are given in Table 9. The first MCDHF CV SrD $nl \geq 6s$ gives electric quadrupole A HFS constants that are near the literature values with at most 14% difference for $A(^2D_{5/2})$. However, the magnetic dipole B constants need more correlations to be accurately determined, as shown by the discrepancies for the D levels ($\approx 50\%$). However, when an experimental value exists, the calculated value agrees with only $\approx 9\%$ difference for the $B(^2P^o_{3/2})$ constant. Adding deeper correlations with the second MCDHF CV SrD $nl \geq 5p$ deteriorates the agreements with the experimental values [37,38] and the other theoretical values [14,39,40] for all the A HFS constants except $A(^2D_{5/2})$. The B HFS constants are 40% closer to the

 doi:10.20944/preprints202607.1297.v1

calculated theoretical values of Sahoo et al. [14] (RCC). The agreement is preserved for the $B(^2P^o_{3/2})$ constant ($\approx 9\%$) but is now too large compared to the experiment value. We are still convinced that adding correlation orbitals with higher l encapsulates the orbital polarization that was neglected in the first MCDHF CV SrD $nl \geq 6s$ strategy and is important for a reliable determination of the B hyperfine constant [24].

After the MCDHF calculations, higher-order core-core (CC) correlations are added using RCI. Like in the Ca II case, two models are considered for each optimization strategy by allowing single and double (SD) substitutions. For all A HFS constants and for each orbital basis, both RCI models (RCI CC SD $nl \geq 6s$ and RCI CC SD $nl \in \{6p, 6s, 5p, 5s\}$) lower the positive values and increase the negative values. However, the added CC correlations are not enough to have a significantly better agreement for the B HFS constants for the D levels while using the MCDHF CV SrD $nl \geq 6s$ orbital basis. The agreement even worsened for the $^2P^o_{3/2}$ level with nearly a 100 MHz difference with the experimental value. Overall, the best agreement is obtained with the MCDHF CV SrD $nl \geq 5p$ + RCI CC SD $nl \in \{6p, 6s, 5p, 5s\}$ strategy. The agreement between the calculated value and RCC value [14] is still satisfactory for the $A(^2D_{5/2})$ constant.

We recall that, for Sr (Z = 38) and Ba (Z = 56), the $A(^2D_{5/2})$ HFS constant was problematic, with an opposite sign between calculated and literature values [16]. For Ra (Z = 88), the HFS constant does not show the same behavior. To understand this more clearly we again move to the non-relativistic formalism, where the magnetic dipole HFS constant A is given as a sum of orbital, spin-dipole, and Fermi contact terms [41]. Table 8 shows the contribution of the different nonrelativistic hyperfine factors on the total A constant. For the Hartree-Fock (HF) calculation, the contact term is zero. Adding core-valence (CV) correlations by opening $6p$ and $6s$ for substitutions to one layer of correlation orbitals $\{7s, 7p, 7d\}$, we see a positive interference for the $^2D_{3/2}$ level and a negative one for the $^2D_{5/2}$ level. Compared with Sr and Ba the negative interference between the different terms is less pronounced for Ra making it less sensitive to neglected higher-order correlation effects from triple (T) and quadruple (Q) substitutions that are the likely causes for the lack of agreement with experiment for the former elements.

Table 8. M1 hyperfine interaction constants A in MHz for $6d\,^2D_{3/2,5/2}$ in ^{223}Ra II. The results at the top are from a HF calculation and the individual contributions from the orbital, spin-dipolar, and Fermi contact terms are shown along with the total value. The results at the bottom are the corresponding values from an MCHF calculation, including CV correlation based on one layer of correlation orbitals.

Level	Term Contribution			
	Orbital	Spin-Dipolar	Contact	Total A
		HF		
$^2D_{3/2}$	46.42	15.49	0.0	61.91
$^2D_{5/2}$	30.95	−4.43	0.0	26.52
		MCHF CV SrD $nl \geq 6s$		
$^2D_{3/2}$	34.26	6.11	30.86	71.23
$^2D_{5/2}$	22.84	−1.75	−30.86	−9.76

 doi:10.20944/preprints202607.1297.v1

Table 9. Magnetic dipole A and electric quadrupole B hyperfine structure constants (in MHz) of ^{223}Ra II ($I = 3/2, \mu = +0.2692\mu_N, Q = 1.22$ b [42]), compared to available theoretical and experimental data. The recommended values are given in the form of $\mu \pm 2\sigma$, exhibiting a 95% confidence level. *: Number of CSFs obtained after reduction using the rcsfginteract_csfg code; [a]: Th. Sahoo et al. (RCC) [14]; [b]: Th. Cserveny et al. (AMPSCI) [40]; [c]: Th. Fei-Chen et al. (RCC) [39]; [d]: Expt. Wendt et al. [37]; [e]: Expt. Neu et al. [38]

Step	$^2S_{1/2}$		$^2D_{3/2}$			$^2D_{5/2}$			$^2P^o_{1/2}$		$^2P^o_{3/2}$		
	N_{CSFs}	A	N_{CSFs}	A	B	N_{CSFs}	A	B	N_{CSFs}	A	N_{CSFs}	A	B
Optimization CV SrD $nl \geq 6s$													
DHF	1	2,811	1	55	272	1	20	288	1	490	1	39	562
MCDHF (+AS1)	70	3,335	156	76	129	184	−35	157	90	620	150	51	732
MCDHF (+AS2)	252	3,408	505	72	194	601	−29	251	289	618	493	61	773
MCDHF (+AS3)	548	3,514	1,052	73	185	1,256	−30	235	604	642	1,038	53	789
MCDHF (+AS4)	958	3,487	1,797	72	185	2,149	−28	238	1,035	640	1,785	50	787
MCDHF (+AS5)	1,482	3,492	2,740	72	184	3,280	−28	235	1,582	642	2,734	52	791
MCDHF (+AS6)	2,120	3,480	3,881	72	184	4,649	−28	235	2,245	638	3,885	52	787
MCDHF (+AS7)	2,872	3,481	5,220	72	185	6,256	−28	236	3,024	638	5,238	52	787
RCI CC SD $nl \geq 6s$ (+AS7)	11,391*	3,222	29,379*	65	234	41,692*	−21	295	11,861*	570	28,513*	47	706
RCI CC SD $nl \in \{6p, 6s, 5p, 5s\}$ (+AS7)	22,774*	3,349	58,750*	66	247	83,376*	−23	379	23,714*	589	57,018*	51	754
RCI CC SD $nl \geq 6s$ (+AS7, NO)	11,391*	3,336	29,379*	67	231	41,692*	−26	297	11,861*	606	28,513*	50	747
RCI CC SD $nl \in \{6p, 6s, 5p, 5s\}$ (+AS7, NO)	22,774*	3,477	58,750*	69	317	83,376*	−26	405	23,714*	627	57,018*	55	806
Optimization CV SrD $nl \geq 5p$													
DHF	1	2,811	1	55	272	1	20	288	1	490	1	39	562
MCDHF (+AS1)	184	3,424	440	80	190	526	−34	234	236	645	404	50	766
MCDHF (+AS2)	680	3,685	1,415	81	328	1,705	−27	418	775	655	1,347	62	836
MCDHF (+AS3)	1,490	3,877	2,944	85	327	3,558	−26	406	1,630	730	2,846	58	922
MCDHF (+AS4)	2,614	3,850	5,027	84	338	6,085	−24	523	2,801	737	4,801	57	932
MCDHF (+AS5)	4,052	3,877	7,664	84	336	9,286	−24	419	4,288	747	7,512	59	942
MCDHF (+AS6)	5,804	3,867	10,855	84	338	13,161	−24	423	6,091	743	10,679	58	937
MCDHF (+AS7)	7,870	3,871	14,600	84	338	17,710	−24	423	8,210	745	14,402	58	940
RCI CC SD $nl \geq 6s$ (+AS7)	16,389*	3,522	38,759*	74	366	53,146*	−18	455	17,047*	650	37,677*	51	823
RCI CC SD $nl \in \{6p, 6s, 5p, 5s\}$ (+AS7)	25,714*	3,583	64,343*	76	365	90,280*	−21	454	26,668*	632	62,303*	54	808
RCI CC SD $nl \geq 6s$ (+AS7, NO)	16,389*	3,583	38,759*	81	396	53,146*	−22	494	17,047*	678	37,677*	54	869
RCI CC SD $nl \in \{6p, 6s, 5p, 5s\}$ (+AS7, NO)	25,714*	3,709	64,343*	81	393	90,280*	−23	492	26,668*	669	62,303*	57	864
This work (LBL)		3,466 ± 331		71 ± 14	306 ± 167		−22 ± 3	417 ± 106		611 ± 61		53 ± 4	781 ± 76
This work (NO), recommended		3,593 ± 328		75 ± 17	355 ± 107		−25 ± 4	449 ± 123		648 ± 59		56 ± 3	835 ± 82
Th.[a]		3,567		77	384		−24	477					
Th.[b]		3,424											
Th.[c]										660		57	
Expt.[d]		3,398.3 ± 2.9								667.1 ± 2.1			
Expt.[d]		3,404 ± 1.9										56.5 ± 8	864.8 ± 1.9

 doi:10.20944/preprints202607.1297.v1

In Ca II, the recommended values for this work were obtained using an NO basis. Following the same approach for Ra II, RCI calculations were repeated, with results presented in Table 9. While the LBL orbital basis remains suitable for the ground level, the NO basis provides better agreement for all excited levels, with an outstanding $< 1\%$ difference with the experimental value of $A(^2P^o_{3/2})$. Nevertheless, the uncertainty calculation for $A(^2S_{1/2})$ encompasses both the NO result and the experimental value.

Nuclear physicists are also interested in ^{225}Ra. Using ^{223}Ra II hyperfine constants in Table 9, the ^{225}Ra II constants are determined thanks to the HFS electronic constants [28]

$$\begin{aligned} A_{\text{el.}} &= A\left(\frac{I}{\mu_I}\right) \\ B_{\text{el.}} &= \frac{B}{Q} \end{aligned} \quad . \tag{22}$$

As $I(^{225}\text{Ra}) = 1/2$ strictly implies that $Q(^{225}\text{Ra}) = 0$ using the Wigner-Eckart theorem [24], only the A hyperfine structure constant can be evaluated for this isotope. Table 10 shows the overall better agreement of the HFS constants calculated with the transformed NO basis as the uncertainties cover literature values.

Table 10. Magnetic dipole A hyperfine structure constants (in MHz) of ^{225}Ra II ($I = 1/2, \mu = -0.730\ \mu_N$) [42], compared to available theoretical and experimental data. The recommended values are given as $\mu \pm 2\sigma$, exhibiting a 95% confidence level. [a]: Th. Sahoo et al. (RCC) [14]; [b]: Th. Skripnikov (RCC) [43]: [c]: Expt. Neu et al. [38]; [d]: Expt. Wendt et al. [37].

Level	This Work (LBL)	This Work (NO)	Th.[a]	Th.[b]	Expt.[c]
$^2S_{1/2}$	$-28{,}555 \pm 2{,}807$	$-30{,}438 \pm 3{,}946$	$-28{,}978$		$-27{,}731 \pm 13^c$
$^2D_{3/2}$	-582 ± 104	-635 ± 138	-626		
$^2D_{5/2}$	167 ± 35	175 ± 35	194		
$^2P^o_{1/2}$	$-5{,}048 \pm 518$	$-5{,}548 \pm 805$		$-5{,}451$	$-5{,}446 \pm 7^d$
$^2P^o_{3/2}$	-447 ± 23	-492 ± 58		-461	-466.4 ± 4.6^c

3.3. Ra I

Neutral radium (Ra I) has two valence electrons. Only a few number of levels have had their HFS experimentally studied. The odd [Rn]$7s7p\ ^3P^o_1$ have been studied by Lynch et al. [44] at the ISOLDE facility and [Rn]$7s7p\ ^3P^o_2$, $^1P^o_1$ have been studied by Wendt et al. [37]. The HFS of the even [Rn]$7s6d\ ^1D_2$, $^3D_{1,2,3}$ levels are only known theoretically. Hassouneh et al. [45] and Bieroń et al. [46] studied them using the MCDHF method, while Dzuba et al. [47] used a Relativistic Hartree-Fock + Configuration Interaction (RHF+CI) method to determine the HFS of ^{213}Ra I ($I = 1/2,\ \mu = 0.6133\ \mu_N$) Their values were used to compute the HFS constants for ^{225}Ra II using eq. (22). The latter two were computationally limited by the number of CSFs or by using a pseudo-relativistic Schrödinger Hamiltonian that could not be enough to study the high relativistic effects of electrons in heavy atoms.

Nezosi et al. [16] Ba I HFS study highlighted that a multireference (MR) is needed for heavy neutral elements such as Ra I while using the MCDHF method. As the main goal of this paper is mainly to transpose Sr II/Ba I-II MCDHF strategies, the configuration that interacts the most with the reference is be added for both studied parities. The even [Rn]$7s6d\ ^1D_2$, $^3D_{1,2,3}$ levels were augmented by a [Rn]$6d^2$ configuration, while the odd [Rn]$7s7p\ ^3P^o_{1,2}$, $^1P^o_1$ levels were augmented by a [Rn]$7p6d$ configuration. Seven correlation layers were considered in Table 11 for the optimization of the MR formed by the two parity configurations.

 doi:10.20944/preprints202607.1297.v1

Table 11. Considered active sets used for the levels studied in ^{223}Ra I.

Correlation layer	$^1D_2$, $^3D_{1,2,3}$, $^1P^o_1$, $^3P^o_{1,2}$
DHF	$\{7s, 7p, 6d, 4f\}$
AS1	$\{8s, 8p, 7d, 5f, 5g\}$
AS2	$\{9s, 9p, 8d, 6f, 6g\}$
AS3	$\{10s, 10p, 9d, 7f, 7g\}$
AS4	$\{11s, 11p, 10d, 8f, 8g\}$
AS5	$\{12s, 12p, 11d, 9f, 9g\}$
AS6	$\{13s, 13p, 12d, 10f, 10g\}$
AS7	$\{14s, 14p, 13d, 11f, 11g\}$

The first calculations were performed in the layer-by-layer (LBL) approach and the results are displayed in Table 12. Due to the two valence-electron structure of Ra I, an additional optimization strategy could be considered based on valence-valence (VV) correlations. Computations shows that the MCDHF VV SrD optimization strategy is not sufficient to take into account the core polarization needed for an accurate determination of the hyperfine structure, with differences ranging from $\approx$ 40MHz for $B(^3D_1)$ to $\approx$ 260 MHz for $B(^3P^o_2)$. Adding core-valence (CV) correlations in the MCDHF VV SrD + CV SrD $nl \geq 6s$ strategy adds the important polarization of the core caused by the valence electrons with already satisfactory agreement with literature values for the A constants. The cost to include these important correlations is to increase the number of CSFs by nearly 70 times for the even levels, add 100 times for the odd levels. One final layer of optimization in MCDHF VV SrD + CV SrD $nl \geq 5d$ was added to match the Ba I [16] model. It again shows that the more correlations, the better, especially for the B hyperfine constants, when asymmetrical d ($5d$) core orbital substitutions are allowed. This behavior was already observed in Ba and reinforces the idea that substitutions from orbitals with a higher l take into account the orbital polarization that was previously neglected and are therefore important for a reliable determination of B [24]. This third layer of optimization increases the HFS constants for all the levels in absolute value.

Adding higher-order correlations with SD substitutions in a RCI step highly increases the number of CSFs to a total of 2 933 035 for the biggest MCDHF VV SrD + CV SrD $nl \geq 5d$ + RCI CC SD $nl \in \{6s, 6p, 5s, 5p\}$ step. Therefore, even if T substitutions are known in Na I to correct CC correlations to the HFS [23], they could not be added in Ra I. Nevertheless, the largest model shows the best agreement for this approach, with only 1 MHz of discrepancy for $B(^3D_2)$, but can still under-perform for $B(^3D_2)$ or $B(^3P^o_{1,2})$ with $\approx$ 60 and $\approx$ 20% difference with literature values, respectively.

Taking the LBL picture as a whole when determining the final values in the $\mu \pm 2\sigma$ format shows satisfactory results for $A(^3D_1)$ with only 2% difference with the latest available MCDHF values [45]. Our calculations are in agreement with the available experimental value for $A(^3P^o_2)$ [37] with $\approx$ 2% discrepency and outperforming Hassouneh et al. [45] MCDHF calculations for this level while giving an uncertainty estimation.

Moving to the NO basis allows us to get an overall better agreement than the LBL calculation, as it was already the case for ^{43}Ca II and ^{223}Ra II. The final values with uncertainty estimates cover other theoretical calculations. When the NO basis degrades the values compared to the LBL basis, it is always only by a few percent. Therefore, these values are the recommended ones for this work.

doi:10.20944/preprints202607.1297.v1

Table 12. Magnetic dipole A and electric quadrupole B hyperfine structure constants (in MHz) of ^{223}Ra I ($I = 3/2, \mu = +0.2692\mu_N, Q = 1.22$ b [42]), compared to available theoretical and experimental data. The recommended values are given in the form of $\mu \pm 2\sigma$, exhibiting a 95% confidence level. *: Number of CSFs obtained after reduction using the rcsfginteract_csfg code; [a]: Th. Hassouneh et al. (MCDHF) [45]; [b]: Th. Bieroń et al. (MCDHF) [46]; [c]: Th. Calculated from Dzuba et al. (RHF+RCI) [47]; [d]: Expt. Lynch et al. [44]; [e]: Expt. Wendt et al. [37]

Strategy	$^3D_1$			$^3D_2$			$^1D_2$		$^3D_3$			$^3P_1^o$			$^1P_1^o$			$^3P_2^o$	
	N_{CSFs}	A	B	N_{CSFs}	A	B	A	B	N_{CSFs}	A	B	N_{CSFs}	A	B	A	B	N_{CSFs}	A	B
Layer-by-layer (LBL)																			
MCDHF VV SrD	626	−458	91	910	292	135	−81	303	898	350	199	635	896	−323	−225	228	852	565	425
RCI CC SD $nl \geq 6s$	85,320*	−559	78	266,206*	272	133	−75	272	189,081*	382	211	172,279*	963	−322	−219	353	320,622*	637	447
RCI CC SD $nl \in \{6s, 6p, 5s, 5p\}$	170,014*	−567	98	531,502*	273	162	−73	320	377,264*	388	264	353,923*	976	−327	−220	375	640,392*	646	459
MCDHF VV SrD + CV SrD $nl \geq 6s$	41,956	−596	70	59,801	367	127	−136	285	65,843	425	188	64,276	1,221	−421	−362	395	91,187	717	625
RCI CC SD $nl \geq 6s$	123,653*	−572	79	322,284*	320	134	−100	250	248,578*	404	209	237,283*	1,059	−344	−274	347	404,447*	666	477
RCI CC SD $nl \in \{6s, 6p, 5s, 5p\}$	208,347*	−583	101	587,580*	320	166	−98	302	436,761*	410	267	413,927*	1,070	−345	−274	371	724,217*	675	483
MCDHF VV SrD + CV SrD $nl \geq 5d$	116,496	−658	129	167,242	421	212	212	396	186,546	477	328	177,207	1385	−477	−416	464	253,427	805	719
RCI CC SD $nl \geq 6s$	197,118*	−623	129	429,417*	364	206	−116	357	355,757*	447	330	349,045*	1,180	−389	−311	404	563,936*	735	548
RCI CC SD $nl \in \{6s, 6p, 5s, 5p\}$	280,602*	−628	129	693,084*	362	204	−113	343	553,300*	449	330	524,247*	1,179	−372	−309	397	881,802*	738	523
Natural orbitals (NO)																			
MCDHF VV SrD	626	−458	91	910	292	135	−81	303	898	350	199	635	896	−323	−225	228	852	565	425
RCI CC SD $nl \geq 6s$	85,320*	−581	77	266,206*	280	134	−76	278	189,081*	398	210	172,279*	1,000	−384	−202	444	320,622*	657	554
RCI CC SD $nl \in \{6s, 6p, 5s, 5p\}$	170,014*	−607	112	531,502*	291	184	−79	369	377,264*	416	298	353,923*	1,048	−407	−208	480	640,392*	691	600
MCDHF VV SrD + CV SrD $nl \geq 6s$	41,956	−599	72	59,801	369	129	−135	290	65,843	427	192	64,276	1,216	−429	−353	410	91,187	714	639
RCI CC SD $nl \geq 6s$	123,653*	−595	80	322,284*	331	136	−104	257	248,578*	420	212	237,283*	1,093	−400	−256	422	404,447*	686	569
RCI CC SD $nl \in \{6s, 6p, 5s, 5p\}$	208,347*	−621	117	587,580*	342	189	−107	354	436,761*	437	305	413,927*	1,138	−421	−262	480	724,217*	718	613
MCDHF VV SrD + CV SrD $nl \geq 5d$	116,496	−664	132	167,242	425	216	−157	403	186,546	481	334	177,207	1,377	−492	−400	494	253,427	800	746
RCI CC SD $nl \geq 6s$	197,118*	−638	147	429,417*	374	231	−119	409	355,757*	459	370	349,045*	1,202	−458	−284	505	563,936*	748	668
RCI CC SD $nl \in \{6s, 6p, 5s, 5p\}$	280,602*	−662	147	693,084*	385	231	−123	400	553,300*	474	370	524,247*	1,237	−450	−292	506	881,802*	776	658
This work (LBL)		−593 ± 63	109 ± 35		318 ± 89	177 ± 46	−95 ± 40	322 ± 41		416 ± 62	287 ± 74		1,075 ± 203	−348 ± 45	−267 ± 89	381 ± 28		686 ± 94	488 ± 65
This work (NO), recommended		−630 ± 57	125 ± 38		339 ± 94	201 ± 52	−103 ± 45	374 ± 47		442 ± 59	324 ± 79		1,141 ± 189	−426 ± 44	−254 ± 85	489 ± 29		728 ± 87	624 ± 61
Th.[a]		−607	130		218	213	−143	388		428	346		1,207	−468	−341	419		622	655
Th.[b]		−612	125		382	210	−140	382		428	346		1,252	−476	−330	419			
Th.[c]		−604			257		−47			403			1,185		−242.3				
Expt.[d]													1,202.5 ± 3.0	−472.1 ± 2.0					
Expt.[e]													1,202.1 ± 0.6	−470.2 ± 1.2	−344.5 ± 0.9	421.5 ± 1.6		699.6 ± 3.3	688.5 ± 4.0

 doi:10.20944/preprints202607.1297.v1

Using our final values for both LBL and NO calculations in ^{223}Ra I and eq. (22), the ^{225}Ra I HFS constants could be determined. With $\mu = 0.271\ \mu_N$ [45], $\mu = 0.2705\ \mu_N$ [46] and $\mu = 0.6133\ \mu_N$ [47], the same has been done with available theoretical values for ^{223}Ra I and ^{213}Ra I isotopes, respectively. All these deduced HFS A constants in ^{225}Ra I are reported in Table 13 along with the available experimental values. The key message learned from Table 13 is that, for most levels, the HFS is hard to compute given the size of the Ra atom. The theoretical uncertainty in our results is in line with the values reported in the literature.

Table 13. Magnetic dipole A hyperfine structure constants (in MHz) of ^{225}Ra I ($I = 1/2, \mu = -0.730\ \mu_N$) [42], compared to available theoretical and experimental data. The recommended values are given as $\mu \pm 2\sigma$, exhibiting a 95% confidence level. [a]: Th. Calculated from Hassouneh et al. (MCDHF) [45]; [b]: Th. Calculated from Bieroń et al. (MCDHF) [46]; [c]: Th. Calculated from Dzuba et al. (RHF+RCI) [47]; [d]: Expt. Guest et al. [48]; [e]: Expt. Wendt et al.[37].

Level	This Work (LBL)	This Work (NO)	Th.[a]	Th.[b]	Th.[c]	Expt.
$^3D_1$	4,848 ± 519	5,152 ± 463	4,905	4,955	4,890	4,687.70 ± 1.5[d]
$^3D_2$	−2,604 ± 726	−2,776 ± 767	−1,763	−3,093	−2,082	
$^1D_2$	774 ± 330	842 ± 364	1,153	1,133	381	
$^3D_3$	−3,401 ± 509	−3,616 ± 482	−3,455	−3,465	−3,266	
$^3P^o_1$	−8,791 ± 1661	−9,330 ± 1,546	−9,751		−9,591	−9,793.90 ± 4.3[e]
$^1P^o_1$	2,186 ± 730	2,077 ± 692	2,757		1,962	2,796.50 ± 1.5[d]
$^3P^o_2$	−5,613 ± 771	−5,955 ± 713	−5,027		−5,519	

4. Conclusions

This work presented a comprehensive computational study of the HFS of low-lying levels in Ca II and Ra I-II, employing the MCDHF and RCI method [8] within the GRASP framework [49] enhanced with Configuration State Function Generators (CSFGs) [27].

Building upon our established models for strontium (Sr) and barium (Ba) [16], we successfully extended this methodology to both a lighter alkaline-earth ion, calcium (Ca), and the heavy radioactive element radium (Ra). The implementation of a NO basis for HFS calculations in heavy elements represented a significant methodological advancement, accounting for orbital relaxation and systematically improving accuracy. Furthermore, we introduced a robust statistical approach for uncertainty estimation, providing experimenters with reliable theoretical bounds for their measurements.

The calcium ion (Ca II) served as a crucial validation case, allowing us to refine our computational approach through detailed analysis of orbital substitution contributions. This investigation revealed the dominant electron correlations influencing HFS and demonstrated that an NO basis induce valence orbital contraction, consistent with observations in lighter elements. Our final values for Ca II exhibited excellent agreement with experimental data while offering precise theoretical uncertainty estimates, thereby confirming the reliability of our method for subsequent applications to more complex systems.

For singly ionized radium (Ra II), we presented the first MCDHF calculations of HFS constants for the [Rn]$6d\ ^2D_{3/2,5/2}$ levels, supplementing existing data for the ground and excited P levels. Despite computational limitations that restricted our correlation analysis to the $3d$ core orbital, we identified $6s$ substitutions as providing the most significant contributions. The NO basis yielded the best agreement with experimental values for the [Rn]$7p\ ^2P^o_{3/2}$ level, with discrepancies below one percent. Our recommended values, complete with uncertainty estimates, encompassed existing theoretical predictions and established essential reference data for future spectroscopic studies. However, unlike other one-valence atomic structures like Sr II and Ba II, the sign change between the final and the experimental value for $A(^2D_{5/2})$ did not appear and, instead, a good agreement is seen with the accurate RCC calculation of Sahoo et al. [14]. A succinct MCHF calculation for the [Rn]$6d\ ^2D_{3/2,5/2}$ levels still showed that this constant might be sensible to interference in the CSFs expansion with cancellation between the non-relativistic orbital and Fermi contact terms.

 doi:10.20944/preprints202607.1297.v1

The neutral radium (Ra I) atom was examined to provide HFS constants critical for determining electric field gradients and interpreting molecular spectra, particularly for RaF. Our calculations for ^{223}Ra I produced electric quadrupole B constants that aligned well with literature values while incorporating uncertainty quantification. The [Rn]$7s6d\ ^3D_2$ and [Rn]$7s7p\ ^3P^o_1$ levels, which are separated by merely 5.41 cm^{-1} and are of particular importance in BSM physics due to their enhanced sensitivity to parity and time-reversal (PT) violating effects, were also studied. The theoretical bounds we provided will guide future experimental and theoretical investigations in this domain.

This HFS investigation marked the first successful application of the newly developed GRASPG [27] code to high-Z elements, demonstrating its capacity to efficiently handle complex atomic systems. Future enhancements, including the integration of partitioned correlation function interaction (PCFI) [50], promise to further improve the precision of hyperfine structure calculations by directly targeting the most significant orbital correlations. Experimental validation of our theoretical models would enable more refined uncertainty estimates. While higher-order substitutions remain computationally intensive, with configuration state function counts already approaching three million for Ra I, natural orbitals emerge as a particularly promising approach. A dedicated study exploring various natural orbital methodologies for second-row elements is currently in progress, highlighting the potential of this approach for atomic structure calculations.

Author Contributions: Conceptualization, L.N. and P.P.; methodology, L.N., P.P., and P.J.; software, P.J.; validation, L.N., P.P., and P.J.; formal analysis, L.N.; investigation, L.N.; resources, L.N. and P.P.; data curation, L.N. and P.P.; writing—original draft preparation, L.N.; writing—review and editing, L.N., P.P., and P.J.; visualization, P.P.; supervision, P.P.; project administration, P.P.; funding acquisition, P.P. All authors have read and agreed to the published version of the manuscript.

Funding: This research was funded by F.R.S.-FNRS–EOS grant number O.0004.22. This project received funding from the FWO and F.R.S.-FNRS under the Excellence of Science (EOS) program (number O.0004.22). Part of the atomic calculations were made with computational resources provided by the Consortium des Equipements de Calcul Intensif (CECI), funded by the F.R.S.-FNRS under grant no. 2.5020.11 and by the Walloon Region of Belgium. P.J. acknowledges support from the Swedish Research Council (VR 2023-05367).

Data Availability Statement: The original contributions presented in this study are included in the article.

Acknowledgments: We would like to thank Prof. Gerda Neyens of KU Leuven (Belgium) for the interesting discussions around the use of Ra in radioactive molecules. P.P. is Research Associate of the Belgian Fund for Scientific Research F.R.S.-FNRS.

Conflicts of Interest: The authors declare no conflicts of interest. The funders had no role in the design of the study; in the collection, analyses, or interpretation of data; in the writing of the manuscript; or in the decision to publish the results.

Abbreviations

The following abbreviations are used in this manuscript:

AMPSCI	Atomic Many-body Perturbation theory in the Screened Coulomb Interaction
AS	Active Set
ASF	Atomic State Function
CC	Core–Core
CSF	Configuration State Function
CSFG	Configuration State Function Generator
CV	Core–Valence
D	Double
DHF	Dirac–Hartree–Fock
GRASP	General Relativistic Atomic Structure Package

 doi:10.20944/preprints202607.1297.v1

HF	Hartree–Fock
HFS	Hyperfine Structure
IS	Isotope Shift
MCDHF	Multiconfiguration Dirac–Hartree–Fock
MCHF	Multiconfiguration Hartree–Fock
MR	MultiReference
NO	Natural Orbital
PCFI	Partitioned Correlation Function Interaction
RCC	Relativistic Coupled Cluster
RCI	Relativistic Configuration Interaction
RHF+CI	Relativistic Hartree–Fock + Configuration Interaction
RMBPT	Relativistic Many-Body Perturbation Theory
S	Single
SD	Single and Double
SrD	Single and restricted Double
SR	Single Reference
VV	Valence–Valence

References

1. Nörtershäuser, W.; Blaum, K.; Icker, K.; Müller, P.; Schmitt, A.; Wendt, K.; Wiche, B. Isotope shifts and hyperfine structure in the $3d\,^2D_J \rightarrow 4p\,^2P_J$ transitions in calcium II. *The European Physical Journal D - Atomic, Molecular and Optical Physics* **1998**, *2*, 33–39. https://doi.org/10.1007/s100530050107.
2. Frebel, A. Observing the r-Process Signature in the Oldest Stars, 2008. https://doi.org/10.48550/ARXIV.0812.1227.
3. Osorio, Y.; Aguado, D.S.; Prieto, C.A.; Hubeny, I.; González Hernández, J.I. Accurate Metallicities for Very Metal-poor Stars from the Ca II Infrared Triplet. *The Astrophysical Journal* **2022**, *928*, 173. https://doi.org/10.3847/1538-4357/ac5a53.
4. Murga, M.; Zhu, G.; Ménard, B.; Lan, T.W. Calcium H & K and sodium D absorption induced by the interstellar and circumgalactic media of the Milky Way. *Monthly Notices of the Royal Astronomical Society* **2015**, *452*, 511–519. https://doi.org/10.1093/mnras/stv1277.
5. Burbidge, E.M.; Burbidge, G.R.; Fowler, W.A.; Hoyle, F. Synthesis of the Elements in Stars. *Reviews of Modern Physics* **1957**, *29*, 547–650. https://doi.org/10.1103/revmodphys.29.547.
6. Quinet, P.; Argante, C.; Fivet, V.; Terranova, C.; Yushchenko, A.V.; Biémont, É. Atomic data for radioactive elements Ra I, Ra II, Ac I and Ac II and application to their detection in HD 101065 and HR 465. *Astronomy & Astrophysics* **2007**, *474*, 307–314. https://doi.org/10.1051/0004-6361:20078082.
7. Pian, E.; D'Avanzo, P.; Benetti, S.; Branchesi, M.; Brocato, E.; Campana, S.; Cappellaro, E.; Covino, S.; D'Elia, V.; Fynbo, J.P.U.; et al. Spectroscopic identification of r-process nucleosynthesis in a double neutron-star merger. *Nature* **2017**, *551*, 67–70. https://doi.org/10.1038/nature24298.
8. Itano, W. Quadrupole moments and hyperfine constants of metastable states of Ca^+, Sr^+, Ba^+, Yb^+, Hg^+ and Au. *Physical Review A* **2006**, *73*. https://doi.org/10.1103/PhysRevA.73.022510.
9. Goble, A.T.; Maleki, S. Measurements of hyperfine constants in Ca^+. *Physical Review A* **1990**, *42*, 649–650. https://doi.org/10.1103/physreva.42.649.
10. Neyens, G., 2026. Private communication.
11. Bieroń, J.; Gaigalas, G.; Gaidamauskas, E.; Fritzsche, S.; Indelicato, P.; Jönsson, P. Multiconfiguration Dirac-Hartree-Fock calculations of the electric dipole moment of radium induced by the nuclear Schiff moment. *Physical Review A* **2009**, *80*. https://doi.org/10.1103/physreva.80.012513.
12. Flambaum, V.V. Enhancement of parity and time invariance violation in the radium atom. *Physical Review A* **1999**, *60*, R2611–R2613. https://doi.org/10.1103/physreva.60.r2611.
13. Versolato, O.O.; Wansbeek, L.W.; Jungmann, K.; Timmermans, R.G.E.; Willmann, L.; Wilschut, H.W. Potential of electric quadrupole transitions in radium isotopes for single-ion optical frequency standards. *Physical Review A* **2011**, *83*. https://doi.org/10.1103/physreva.83.043829.
14. Sahoo, B.K.; Das, B.P.; Chaudhuri, R.K.; Mukherjee, D.; Timmermans, R.G.E.; Jungmann, K. Investigations of Ra^+ properties to test possibilities of new optical frequency standards. *Physical Review A* **2007**, *76*. https://doi.org/10.1103/physreva.76.040504.

 doi:10.20944/preprints202607.1297.v1

15. Sahoo, B.K.; Jönsson, P.; Gaigalas, G. Comparative Analysis of Mg^+ Properties using Multiconfiguration Dirac-Hartree-Fock and Relativistic Coupled-Cluster Methods. *Physical Review A* **2025**, *112*. https://doi.org/10.1103/bpg7-wm48.
16. Nezosi, L.; Maison, L.; Palmeri, P.; Jönsson, P.; Godefroid, M. Study of the Hyperfine Structure of Sr II, Ba I and Ba II: An MCDHF Approach for Modeling the Low-Lying Levels. *Atoms* **2026**, *14*, 17. https://doi.org/10.3390/atoms14030017.
17. Froese Fischer, C.; Gaigalas, G.; Jönsson, P.; Bieroń, J. GRASP2018—A Fortran 95 version of the General Relativistic Atomic Structure Package. *Computer Physics Communications* **2019**, *237*, 184–187. https://doi.org/10.1016/j.cpc.2018.10.032.
18. Atalay, B. Relativistic multiconfiguration calculations of energy levels, transition rates and hyperfine constants in neutral indium. *Journal of Quantitative Spectroscopy and Radiative Transfer* **2026**, *352*, 109812. https://doi.org/10.1016/j.jqsrt.2026.109812.
19. Grant, I.P. *Relativistic quantum theory of atoms and molecules*; Springer Series on Atomic, Optical, and Plasma Physics, Springer, 2007.
20. Jönsson, P.; Godefroid, M.; Gaigalas, G.; Ekman, J.; Grumer, J.; Li, W.; Li, J.; Brage, T.; Grant, I.P.; Bieroń, J.; et al. An Introduction to Relativistic Theory as Implemented in GRASP. *Atoms* **2022**, *11*, 7. https://doi.org/10.3390/atoms11010007.
21. Lindgren, I.; Lindgren, J.; Mårtensson, A.M. Many-body calculations of the hyperfine interaction of some excited states of alkali atoms, using approximate Brueckner or natural orbitals. *Zeitschrift für Physik A Atoms and Nuclei* **1976**, *279*, 113–125.
22. Schiffmann, S.; Li, J.; Ekman, J.; Gaigalas, G.; Godefroid, M.; Jönsson, P.; Bieroń, J. Relativistic radial electron density functions and natural orbitals from GRASP2018. *Computer Physics Communications* **2022**, *278*, 108403. https://doi.org/10.1016/j.cpc.2022.108403.
23. Schiffmann, S.; Godefroid, M.; Ekman, J.; Jönsson, P.; Fischer, C.F. Natural orbitals in multiconfiguration calculations of hyperfine-structure parameters. *Physical Review A* **2020**, *101*. https://doi.org/10.1103/PhysRevA.101.062510.
24. Lindgren, I.; Morrison, J. *Atomic Many-Body Theory*; Springer Berlin Heidelberg, 1986. https://doi.org/10.1007/978-3-642-61640-2.
25. Froese Fischer, C.; Gaigalas, G.; Jönsson, P.; Bieroń, J. GRASP—2018 — A Fortran 95 version of the General Relativistic Atomic Structure Package. *Comput. Phys. Commun.* **2019**, *237*, 184–187. https://doi.org/10.1016/j.cpc.2018.10.032.
26. Jönsson, P.; Gaigalas, G.; Fischer, C.F.; Bieroń, J.; Grant, I.P.; Brage, T.; Ekman, J.; Godefroid, M.; Grumer, J.; Li, J.; et al. GRASP Manual for Users. *Atoms* **2023**, *11*, 68. https://doi.org/10.3390/atoms11040068.
27. Si, R.; Li, Y.; Wang, K.; Chen, C.; Gaigalas, G.; Godefroid, M.; Jönsson, P. GRASPG – An extension to GRASP2018 based on configuration state function generators. *Comput. Phys. Commun.* **2025**, *312*, 109604. https://doi.org/10.1016/j.cpc.2025.109604.
28. Papoulia, A.; Schiffmann, S.; Bieroń, J.; Gaigalas, G.; Godefroid, M.; Harman, Z.; Jönsson, P.; Oreshkina, N.S.; Pyykkö, P.; Tupitsyn, I.I. Ab initio electronic factors of the $5s^2 5p 6s\ ^{1,3}P^o_1$ states in Sn I. *Physical Review A* **2021**, *103*. https://doi.org/10.1103/PhysRevA.103.022815.
29. Kondev, F.; Wang, M.; Huang, W.; Naimi, S.; Audi, G. The NUBASE2020 evaluation of nuclear physics properties *. *Chinese Physics C* **2021**, *45*, 030001. https://doi.org/10.1088/1674-1137/abddae.
30. Silverans, R.E.; Vermeeren, L.; Neugart, R.; Lievens, P. Hyperfine structure constants of the CaII states $4s^2 S_{1/2}$ and $4p^2 P_{1/2,3/2}$ and the nuclear quadrupole moment of ^{43}Ca. *Zeitschrift für Physik D Atoms, Molecules and Clusters* **1991**, *18*, 351–356. https://doi.org/10.1007/bf01426597.
31. Yu, K.z.; Wu, L.j.; Gou, B.c.; Shi, T.y. Calculation of the hyperfine structure constants in $^{43}Ca^+$ and $^{87}Sr^+$. *Physical Review A* **2004**, *70*. https://doi.org/10.1103/physreva.70.012506.
32. Sahoo, B.K.; Das, B.P.; Chaudhuri, R.K.; Mukherjee, D. Theoretical studies of the $6s\ ^2S_{1/2} \rightarrow 5d\ ^2D_{3/2}$ parity-nonconserving transition amplitude in Ba^+ and associated properties. *Physical Review A* **2007**, *75*. https://doi.org/10.1103/physreva.75.032507.
33. Bieroń, J.; Filippin, L.; Gaigalas, G.; Godefroid, M.; Jönsson, P.; Pyykkö, P. *Ab initio* calculations of the hyperfine structure of zinc and evaluation of the nuclear quadrupole moment Q (^{67}Zn). *Physical Review A* **2018**, *97*. https://doi.org/10.1103/PhysRevA.97.062505.
34. Bieroń, J.; Froese Fischer, C.; Indelicato, P.; Jönsson, P.; Pyykkö, P. Complete-active-space multiconfiguration Dirac-Hartree-Fock calculations of hyperfine-structure constants of the gold atom. *Physical Review A* **2009**, *79*. https://doi.org/10.1103/PhysRevA.79.052502.

 doi:10.20944/preprints202607.1297.v1

35. IAEA. Nuclear values of interest for Ca. (Consulted Mar. 10th, 2025), https://doi.org/10.1016/j.nima.2015.10.096.
36. R. Jonhson, W. *Atomic Structure Theory*; Springer Berlin Heidelberg, 2007. https://doi.org/10.1007/978-3-540-68013-0.
37. Wendt, K.; Ahmad, S.A.; Klempt, W.; Neugart, R.; Otten, E.W.; Stroke, H.H. On the Hyperfine Structure and Isotope Shift of Radium. *Zeitschrift für Physik D Atoms, Molecules and Clusters* **1987**, *4*, 227–241. https://doi.org/10.1007/bf01436633.
38. Neu, W.; Neugart, R.; Otten, E.W.; Passler, G.; Wendt, K.; Fricke, B.; Arnold, E.; Kluge, H.J.; Ulm, G. Quadrupole moments of radium isotopes from the $7p\ ^2P_{3/2}$ hyperfine structure in Ra II. *Zeitschrift für Physik D Atoms, Molecules and Clusters* **1988**, *11*, 105–111. https://doi.org/10.1007/bf01444425.
39. Li, F.C.; Tang, Y.B.; Qiao, H.X.; Shi, T.Y. Ab initio caclulations of the hyperfine structure of Ra^+ and evaluations of the electric quadrupole moment Q of ^{209,211,221,223}Ra nuclei. *Journal of Physics B: Atomic, Molecular and Optical Physics* **2021**, *54*, 145004. https://doi.org/10.1088/1361-6455/ac1329.
40. Cserveny, R.B.; Roberts, B.M. Theoretical characterization of the barium ii and radium ii ions. *Physical Review A* **2025**, *112*. https://doi.org/10.1103/1rtb-8ymc.
41. Froese Fischer, C. *The Hartree-Fock Method for Atoms: A Numerical Approach*; John Wiley and Sons, 1977.
42. IAEA. Nuclear values of interest for Ra. (Consulted Apr. 10th, 2026), https://doi.org/10.1016/j.nima.2015.10.096.
43. Skripnikov, L.V. Nuclear magnetization distribution effect in molecules: Ra^+ and RaF hyperfine structure. *The Journal of Chemical Physics* **2020**, *153*. https://doi.org/10.1063/5.0024103.
44. Lynch, K.M.; Wilkins, S.G.; Billowes, J.; Binnersley, C.L.; Bissell, M.L.; Chrysalidis, K.; Cocolios, T.E.; Goodacre, T.D.; de Groote, R.P.; Farooq-Smith, G.J.; et al. Laser-spectroscopy studies of the nuclear structure of neutron-rich radium. *Physical Review C* **2018**, *97*. https://doi.org/10.1103/physrevc.97.024309.
45. Hassouneh, O.; Salah, W. Relativistic calculations of the Landé g_J-factors, and hyperfine parameters in Ra-223 isotope. *The European Physical Journal Plus* **2022**, *137*. https://doi.org/10.1140/epjp/s13360-022-02422-2.
46. Bieroń, J. Multiconfiguration Dirac–Hartree–Fock calculations of the hyperfine structures of radium. *Journal of Physics B: Atomic, Molecular and Optical Physics* **2005**, *38*, 2221–2228. https://doi.org/10.1088/0953-4075/38/13/014.
47. Dzuba, V.A.; Flambaum, V.V.; Ginges, J.S.M. Calculation of parity and time invariance violation in the radium atom. *Physical Review A* **2000**, *61*. https://doi.org/10.1103/physreva.61.062509.
48. Guest, J.R.; Scielzo, N.D.; Ahmad, I.; Bailey, K.; Greene, J.P.; Holt, R.J.; Lu, Z.T.; O'Connor, T.P.; Potterveld, D.H. Laser Trapping of ^{225}Ra and ^{226}Ra with Repumping by Room-Temperature Blackbody Radiation. *Physical Review Letters* **2007**, *98*. https://doi.org/10.1103/physrevlett.98.093001.
49. Dyall, K.; Grant, I.; Johnson, C.; Parpia, F.; Plummer, E. GRASP: A general-purpose relativistic atomic structure program. *Computer Physics Communications* **1989**, *55*, 425–456. https://doi.org/10.1016/0010-4655(89)90136-7.
50. Wu, S.; Si, R.; Chen, C.; Gaigalas, G.; Godefroid, M.; Jönsson, P., 2026. Private communication, in preparation for Computer Physics Communications.